

1 **Turbidity maximum zone index: A novel model for remote** 2 **extraction of turbidity maximum zone in different estuaries**

3 Chongyang Wang^{1,3‡}, Li Wang^{1‡}, Danni Wang², Dan Li¹, Chenghu Zhou^{1,3,4}, Hao Jiang¹,
4 Qiong Zheng^{1,5}, Shuisen Chen¹, Kai Jia¹, Yangxiaoyue Liu⁴, Ji Yang^{1,3}, Xia Zhou¹ and
5 Yong Li^{1,3}

6 ¹ Guangdong Open Laboratory of Geospatial Information Technology and Application, Key Lab of
7 Guangdong for Utilization of Remote Sensing and Geographical Information System, Guangzhou
8 Institute of Geography, Guangdong Academy of Sciences, Guangzhou 510070, China

9 ² Guangzhou Xinhua University, Guangzhou 510520, China

10 ³ Southern Marine Science and Engineering Guangdong Laboratory (Guangzhou), Guangzhou
11 511458, China

12 ⁴ State Key Laboratory of Resources and Environmental Information System, Institute of
13 Geographic Sciences and Natural Resources Research, Chinese Academy of Sciences, Beijing
14 100101, China

15 ⁵ Department of Geomatics Engineering, School of Traffic & Transportation Engineering, Changsha
16 University of Science & Technology, Changsha, 410114, China

17 ‡ Equally contributed to this work

18 **Correspondence:** Dan Li (lidan@gdas.ac.cn); Chenghu Zhou (zhouch@lreis.ac.cn)

19 **Abstract.** An efficient recognition and extraction of the estuarine turbidity maximum
20 zone (TMZ) is important for studying terrestrial hydrological processes. Although
21 many studies relevant to TMZ have been conducted worldwide, the extraction methods
22 and criteria used to describe TMZ vary significantly both spatially and temporally. To
23 improve the applicability of the methods adopted in previous studies and to develop a
24 novel model to accurately extract TMZ in multiple estuaries and different seasons from

25 remote sensing imageries, this study estimated the total suspended solids (TSS) and
26 chlorophyll a (Chla) concentrations in three estuaries. These were the Pearl River
27 Estuary (PRE), the Hanjiang River Estuary (HRE), and the Moyangjiang River Estuary
28 (MRE) of Guangdong Province, China. The spatial distribution characteristics of the
29 TSS and Chla concentrations were analyzed. A nearly opposite association was found
30 between the TSS and Chla concentrations in the three estuaries, particularly in the PRE.
31 The regions with high (low) TSS concentrations had relatively low (high) Chla
32 concentrations and therefore, a turbidity maximum zone index (TMZI), defined as the
33 ratio of the difference and sum of the logarithmic transformation of the TSS and Chla
34 concentrations, was firstly proposed. By calculating the TMZI values in the PRE on
35 November 20, 2004 (low-flow season), it was found that the criterion ($TMZI > 0.2$)
36 could be used to identify the TMZs of the PRE effectively. The TMZ extraction results
37 were generally consistent with the visual interpretation results. The area-based accuracy
38 measures showed that the quality (Q) of the extraction reached 0.8429. The same
39 criterion was applied in the PRE on October 18, 2015 (high-flow season), and high
40 accuracy and consistency across seasons were observed ($Q = 0.8171$). The western
41 shoal of the PRE was the main distribution area of TMZs. Extracting TMZs by the
42 newly proposed index performed well in different estuaries and on different dates (HRE
43 on August 13, 2008 in the high-flow season and MRE on December 6, 2013 in the low-
44 flow season). Compared to the previous fixed threshold of TSS or turbidity methods,
45 extracting TMZ using TMZI had higher accuracy and better applicability (Q: 0.1046–

46 0.4770 vs. 0.8171–0.8429). Evidently, this unified TMZI is potentially an optimized
47 method for the global monitoring and extraction of TMZs of estuaries from different
48 satellite remote sensing imageries. It can be used to help the understanding of the spatial
49 and temporal variation of TMZs and estuarine processes at regional and global scales,
50 as well as improve the management and sustainable development of regional society
51 and the natural environment.

52 Keywords: turbidity maximum zone; turbidity maximum zone index; total suspended
53 solid; chlorophyll a; remote sensing; estuary

54 **1 Introduction**

55 The turbidity maximum zone (TMZ) is the dynamic turbid water area within an
56 estuary, where the suspended solid concentrations, namely, sediment and matter, are
57 consistently and significantly higher than landward and seaward (Shen, 1995; Gebhardt
58 et al., 2005; Yu et al., 2014; Li et al., 2019). It is a special phenomenon of suspended
59 sediment movement and migration in estuaries worldwide (Schubel, 1968; Shi et al.,
60 1993; Mitchell et al., 2012; Wang et al., 2021). The spatial distributions and dynamic
61 changes of TMZs not only have a deep and wide impact on the formation and
62 development of estuary morphology, channels, shoals, and sandbars (Asp et al., 2018;
63 Azhikodan and Yokoyama, 2019; Li et al., 2019), but also significantly affect the
64 physics and geochemical and biogeochemical processes of natural estuarine
65 environments, as well as social production activities (Gebhardt et al., 2005; Jalón-Rojas

66 et al., 2016; Kitheka et al., 2016; Toubanc et al., 2016; Yan et al., 2020). TMZ has long
67 been a popular area for scientific study and engineering innovations among researchers,
68 government agencies, engineering corporations, and communities (Shen et al., 2001;
69 Shi et al., 2017; Jiang et al., 2019; Wang et al. 2021).

70 Previous studies have examined TMZ from various aspects based on different data
71 resources and methods, such as the characteristics and dynamics of total suspended
72 solids (TSS) concentrations in TMZ (Yang et al., 2014; Wan and Wang, 2017; Grasso
73 et al., 2018), the mechanisms and formation of TMZ (Brenon and Hir, 1999; Wai et al.,
74 2004; Yu et al., 2014; Toubanc et al., 2016), the location, distribution, and change of
75 TMZ across time (Jiang et al., 2013; Jalón-Rojas et al., 2016; Li et al., 2019; Yan et al.,
76 2020), the interaction with other factors, and its long-term trend (Gebhardt et al., 2005;
77 Chen et al., 2016; Li et al., 2019). The location of TMZ in an estuary is a fundamental
78 question and an important aspect of studying TMZ. It was found that there were two
79 major ways to obtain the locations and distributions of TMZs (Wang et al., 2021). One
80 was a relatively approximate description, such as TMZ locations corresponding to the
81 front of the salinity wedge and moving range of stagnation points, or a distance from
82 coastlines (Feng et al., 2002; Mitchell, 2013; Kitheka et al., 2016; Liu et al., 2016;
83 Toubanc et al., 2016; Gong et al., 2017; Zhang et al., 2019; Yan et al., 2020). The other
84 was a relatively quantitative result. The thresholds of TSS concentrations or turbidity
85 criteria were used to extract the distribution of TMZs (Jiang et al., 2013; Yang and Liu,
86 2015; Chen et al., 2016; Jalón-Rojas et al., 2016; Shi et al., 2017; Li et al., 2019).

87 However, the fixed threshold method has potential drawbacks. It is a challenging task
88 to precisely generate TMZ extraction results at different times using a fixed threshold
89 of TSS concentration because TSS concentrations showed significant variations in
90 different seasons. Moreover, the threshold values are difficult to transfer from local
91 regions to other regions because research and a scientific basis are lacking. The
92 threshold method and criteria vary significantly in different estuaries, in different
93 regions of the same estuary, in the same estuary at different times, and by different
94 studies, demonstrating considerable subjectivity. The results were not comparable
95 ([Wang et al., 2021](#)).

96 TSS concentrations in the TMZs and adjacent waters vary significantly ([Uncles et](#)
97 [al., 2000](#); [Park et al., 2008](#); [Mitchell, 2013](#); [Wang et al., 2018](#)). Many studies have
98 shown that suspended solids can affect the growth of chlorophyll a (Chla) through
99 absorption and sunlight scattering in water ([Pozdnyakov et al., 2005](#); [Chen et al., 2015](#);
100 [Montanher et al., 2014](#); [Wang et al., 2017a](#); [Wang et al., 2020b](#)). Therefore, it was
101 concluded that there is a relationship between TSS concentrations and Chla
102 concentrations and different characteristics in TMZ and normal water bodies in
103 estuaries. This relationship might be used to overcome the drawbacks of previous
104 methods of extracting TMZ and distinguish and recognize TMZ effectively.

105 Based on this analysis, the objectives of this study are to propose a new model
106 with better adaptability and robustness for distinguishing and extracting TMZ in
107 different estuaries and in different seasons. To achieve this goal, the TSS and Chla

108 concentrations in the Pearl River Estuary (PRE), Hanjiang River Estuary (HRE), and
109 Moyangjiang River Estuary (MRE) were first estimated. The different spatial
110 characteristics were analyzed and compared. Subsequently, the corresponding
111 relationship and special features of TSS and Chla concentrations were used to develop
112 a turbidity maximum zone index (TMZI). Finally, the TMZs in these estuaries were
113 extracted at different times by the model (TMZI) and validated and assessed for
114 accuracy.

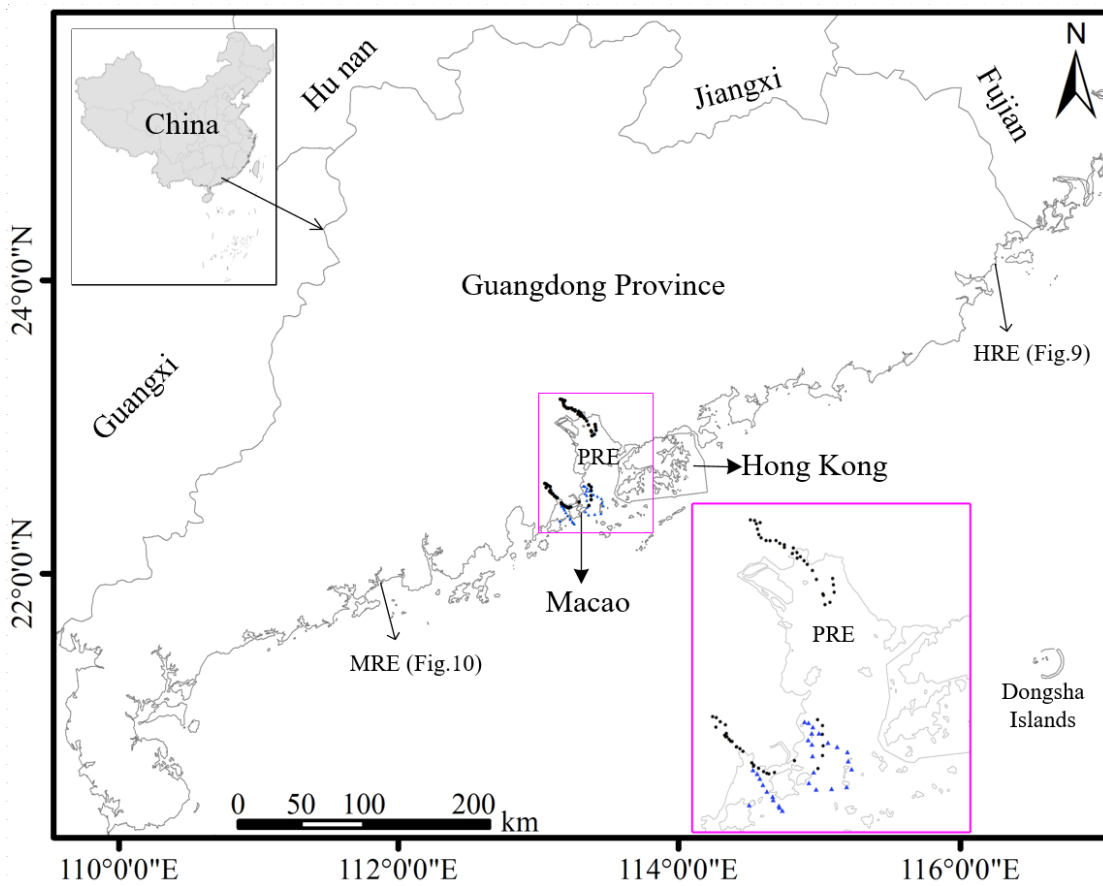
115 The remainder of this paper is organized as follows. The study areas, in situ data,
116 satellite imagery, TSS concentration data, Chla retrieval model, and its calibration and
117 validation are described in [Section 2](#), as well as the TMZ extraction accuracy
118 assessment measures. The spatial analysis of TSS concentration, Chla concentration,
119 and the corresponding relationship between them are presented in [Section 3.1](#). The
120 establishment of TMZI and its application and assessment in different estuaries and at
121 different times are shown in [Sections 3.2-3.5](#). The summary and conclusions are
122 presented in [Section 4](#).

123 **2 Dataset and methods**

124 **2.1 Study areas**

125 The study areas include the Pearl, Hanjiang, and Moyangjiang River Estuaries of
126 Guangdong Province, South China ([Figs. 1, 4, and 7-10](#)). The PRE (horn-shaped) is
127 located between longitudes 113.45 °E and 114.2 °E and latitudes 22.25 °N and 22.85 °N, mainly in

128 the core zone of Guangdong-Hong Kong-Marco Greater Bay Area. The HRE (forking-
 129 shaped) is located between longitudes 116.6 °117 °E and latitudes 23.2 °23.6 °N, mainly
 130 in Shantou city, Eastern Guangdong Province. The MRE (calabash-shaped) is located
 131 between longitudes 111.9 °112.3 °E and latitudes 21.66 °21.8 °N, mainly in Yangjiang
 132 city, Western Guangdong Province.



133
 134 **Fig. 1.** Study areas (PRE, HRE, and MRE) and the locations of the in-situ data indicated by black
 135 dots and blue triangles.

136 The Pearl River has the second largest annual runoff and is the third largest river
 137 in China. The Hanjiang and Moyangjiang Rivers are the second and third largest rivers
 138 in Guangdong Province (Chen et al., 2011; Wang et al., 2018; Wang et al., 2020a).
 139 Previous studies have reported that the sediment loads of the Pearl, Hanjing and

140 Moyangjiang Rivers were $7.53 \cdot 10^7$, $6.93 \cdot 10^6$ and $3.27 \cdot 10^5$ ton per year, respectively
141 (Wang et al., 2017a, b; Wang et al., 2020a). It was found that the three rivers and
142 estuaries have different characteristics, and much associated research has been
143 conducted in these regions for a long time.

144 **2.2 In-situ and satellite data**

145 The 89 in-situ samples, including water surface reflectance and Chla
146 concentrations, were collected from the PRE (Fig. 1, Table 1). Sixty of these samples
147 were also used in a previous study by the current authors (black dots) (Chen et al., 2011).
148 The present study included 29 new samples (blue triangles). Here, these samples were
149 used to recalibrate and validate a Landsat-based Chla concentration retrieval model.

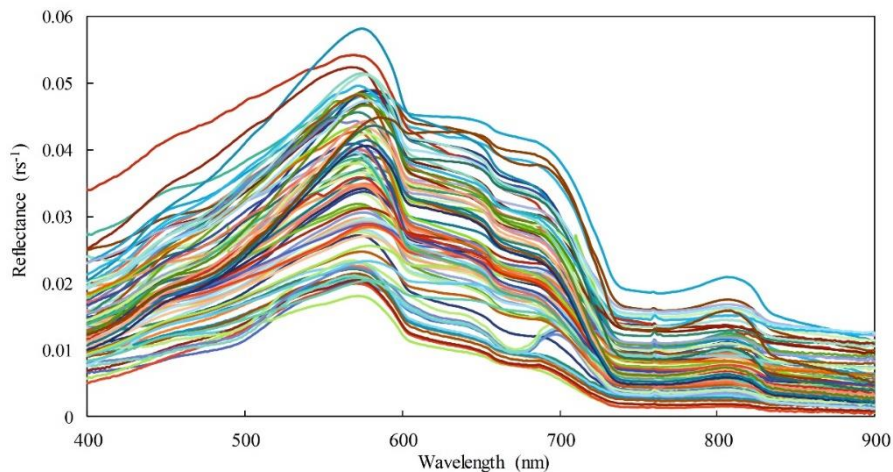
150 In addition, four scenes of good quality Landsat imageries were used. Two images
151 from TM and OLI (path/row = 122/44) were captured on November 20, 2004
152 (ProductID: LT05_L1TP_122044_20041120_20161129_01_T1), and October 18,
153 2015 (LC08_L1TP_122044_20151018_20170403_01_T1), respectively, covering the
154 PRE (Figs. 7a and 8c). The image from TM (path/row = 120/44) was captured on
155 August 13, 2008 (LT05_L1TP_120044_20080813_20161030_01_T1), covering the
156 HRE (Fig. 9c). The final image from OLI (path/row = 123/45), was captured on
157 December 6, 2013 (LC08_L1TP_123045_20131206_20170428_01_T1), covering the
158 MRE (Fig. 10c).

159 **Table 1**

160 The 89 in-situ data.

Date	Samples	Measurements	
Dec 9, 2006	16	Reflectance, Chla	
Dec 21, 2006	12	Reflectance, Chla	Same as
Dec 27, 2007	15	Reflectance, Chla	Chen et al. (2011)
Dec 31, 2007	17	Reflectance, Chla	
Nov 2, 2012	18	Reflectance, Chla	Newly added
Sep 10, 2013	11	Reflectance, Chla	

161



162

163 **Fig. 2.** Remote sensing reflectance of surface water of the 89 in situ data.

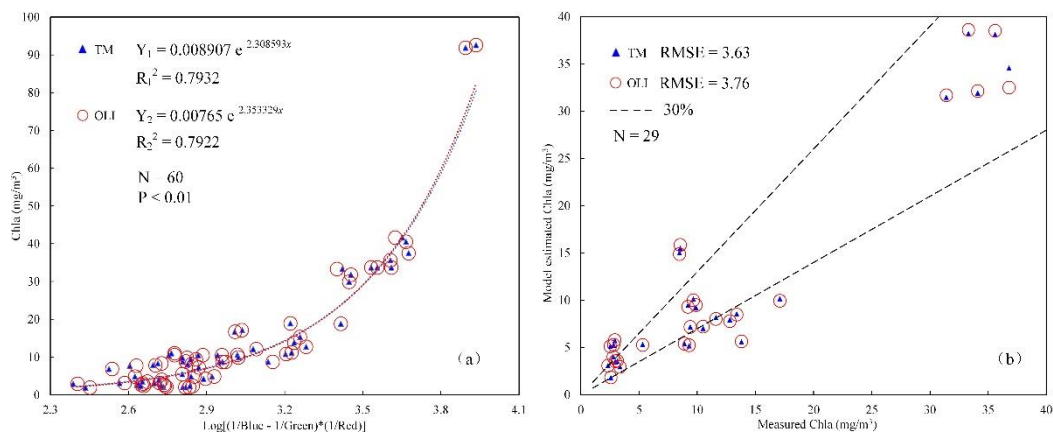
164 **2.3 Total suspended solids data and chlorophyll a data**

165 The aim of this study was to establish and develop a new model (TMZI) based on

166 TSS concentrations and Chla concentrations, and further extract TMZs in three

167 estuaries of Guangdong Province. Therefore, the TSS and Chla concentrations in the

168 study areas were first calculated. The TSS concentration data were obtained from
 169 previous work of the current authors (Wang et al., 2017a, b; Wang et al., 2018; Wang et
 170 al., 2020a). The corresponding Chla data required retrieval using Landsat imagery.
 171 Consequently, a Landsat-based Chla concentration retrieval model was expected to be
 172 suitable for different estuaries. Many models have been developed to estimate Chla
 173 concentration from different remote sensing data (Gregg and Casey, 2004; Chen et al.,
 174 2011; Kim et al., 2016a, b; Attila et al., 2018). Following the features and forms of
 175 some typical chlorophyll a retrieval models (Le et al., 2009; Chen et al., 2011; Le et al.,
 176 2013; Song et al., 2013), a three-band Landsat-based chlorophyll a model using the 89
 177 in-situ samples was recalibrated and validated (Fig. 3; Equation 1). The model, based
 178 on Landsat TM and OLI sensors, explained approximately 80% of the Chla
 179 concentration variation (Chla: 1.92-92.6 mg/m³, N=60, P-value<0.01) and had an
 180 acceptable validation accuracy (Chla: 2.33-36.8 mg/m³, RMSE ≤ 3.76 mg/m³, N=29).



181
 182 **Fig. 3.** The calibration (a) and validation (b) results of the Chla retrieval models based on 89 in situ
 183 data for Landsat sensors.

184
$$Chla = a * e^{b * \text{Log}_{(10)}[\frac{1}{R_1} - \frac{1}{R_2}] * \frac{1}{R_3}} \quad (1)$$

185 where R_1 , R_2 and R_3 represent the blue, green, and red band of the TM and OLI
 186 sensors, respectively. The parameters a and b corresponding to the TM and OLI sensors
 187 are 0.008907, 2.308593 and 0.00765, 2.353329, respectively. The unit of chlorophyll a
 188 concentration is in mg/m^3 .

189 2.4 Accuracy assessment measures

190 To evaluate TMZI extraction accuracy and compare the performances of the
 191 different methods, the common accuracy measures of object recognition in remote
 192 sensing, area-based accuracy measures (Cai et al., 2018), was used.

193 Suppose that A_E is the area of the extracted TMZ, A_C is the correct part of A_E , and
 194 A_R is the reference TMZ. Then the quality (Q) of the TMZ extraction results in the study
 195 could be defined as follows (equation 2).

196
$$Q = \frac{A_C}{A_E + A_R - A_C} \quad (2)$$

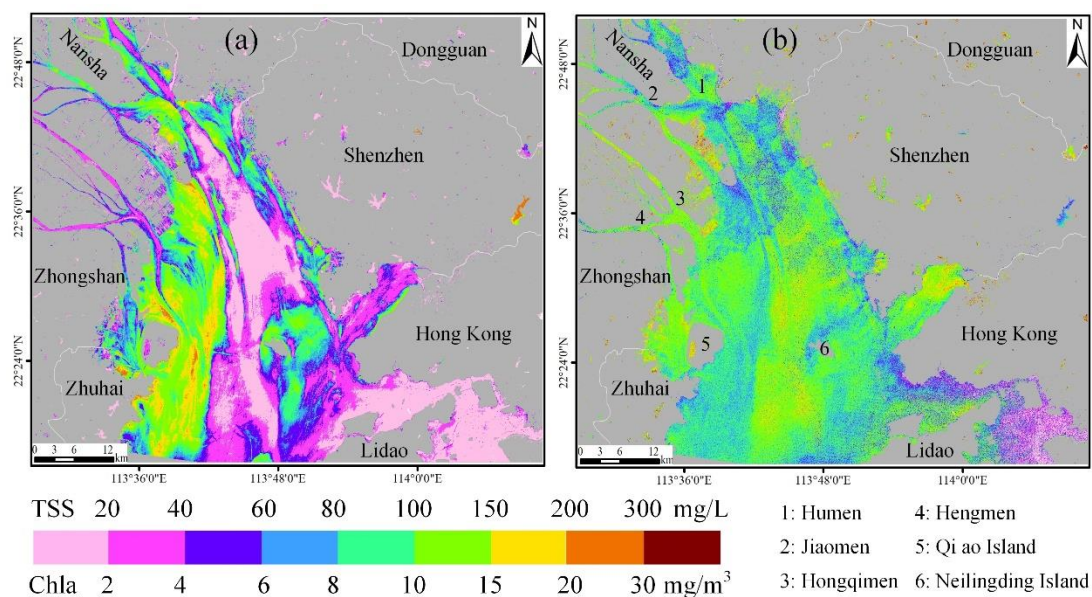
197 The range of Q is 0 to 1. The bigger the Q value, the higher the accuracy of the
 198 TMZ extraction results, and the better performance of the method.

199 3 Results and discussion

200 3.1 The spatial characteristics of TSS and Chla concentrations in 201 estuaries

202 Chla concentrations in each estuary were estimated using the Chla concentration
 203 retrieval model that was developed (Fig. 3). The different spatial distribution
 204 characteristics of the TSS and Chla concentrations were analyzed. Taking the PRE as

205 an example, TSS concentrations in the low-flow season of the PRE (November 20,
 206 2004) have a large variation ranging from 1.37 mg/L to more than 200 mg/L (Fig. 4a).
 207 Due to the strong interaction between runoff and tide, the main region of high TSS
 208 concentrations is in the west shoal of the PRE (Wang et al., 2018), where concentrations
 209 of more than 100 mg/L were frequently found. In addition, TSS concentrations in parts
 210 of the east shoal and Neilingding island adjacent waters were also relatively higher. The
 211 other areas of the PRE have low TSS concentrations, where the maximum value is
 212 generally not more than 40 mg/L, particularly in the Hong Kong coastal water bodies
 213 (Fig. 4a).



214
 215 **Fig. 4.** The estimated TSS concentrations (a) and Chla concentrations (b) in the PRE on November
 216 20, 2004.

217 In contrast to the TSS concentration results, the Chla concentrations in the PRE
 218 have significantly lower values of less than 20 mg/m³ in almost the entire PRE (Fig.
 219 4b). The results concord with the findings of Liu et al. (2017) and Huang et al. (2005),

220 who found that Chla concentrations ranged from 0.24 mg/m³ to 21.5 mg/m³ in the PRE
221 at different times. Furthermore, Chla concentrations in the PRE show almost opposite
222 spatial characteristics to TSS concentrations. Apart from the eastern Lidao district
223 coastal water bodies, the regions of relatively high (low) Chla concentrations are the
224 regions of relatively low (high) TSS concentrations. These corresponding features are
225 apparent in the four waterways, namely, Humen, Jiaomen, Hongqimen, and Hengmen
226 waterways and the shoals, and channels of the PRE (Fig. 4).

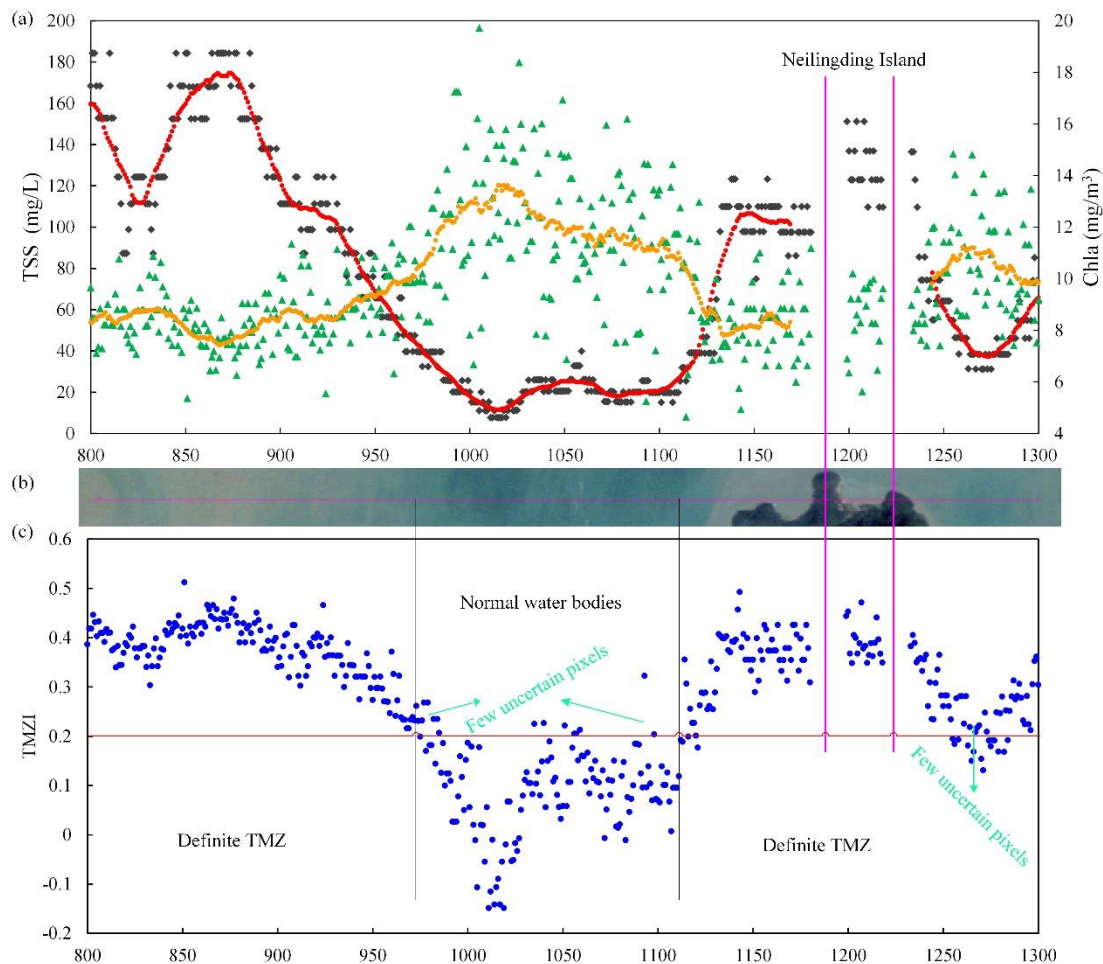
227 To further analyze and assess the corresponding relationship between TSS and
228 Chla concentrations in the estuaries, three rows of TSS and Chla concentration values
229 in the PRE were extracted (Fig. 7a; pink lines; rows 1200, 1600, and 1900, columns
230 from 800 to 1300). The results for row 1600 are shown in Fig. 5(a). A correlation
231 analysis showed a significant negative correlation between TSS and Chla
232 concentrations. For the original TSS and Chla concentrations, the correlation
233 coefficient was -0.6531. The correlation coefficient reaches approximately -0.9 for its
234 trend lines (Fig. 5a).

235 **3.2 Establishment and application of TMZI**

236 Based on the analysis and corresponding features between TSS and Chla
237 concentrations, it is considered that the transform results derived from the two water
238 color elements may help to better distinguish and extract TMZ. In this study, TMZI was
239 defined as the ratio of the difference and sum of logarithmic transformation of TSS

240 concentrations and Chla concentrations (equation 3), which is similar to the normalized
 241 difference vegetation index (NDVI).

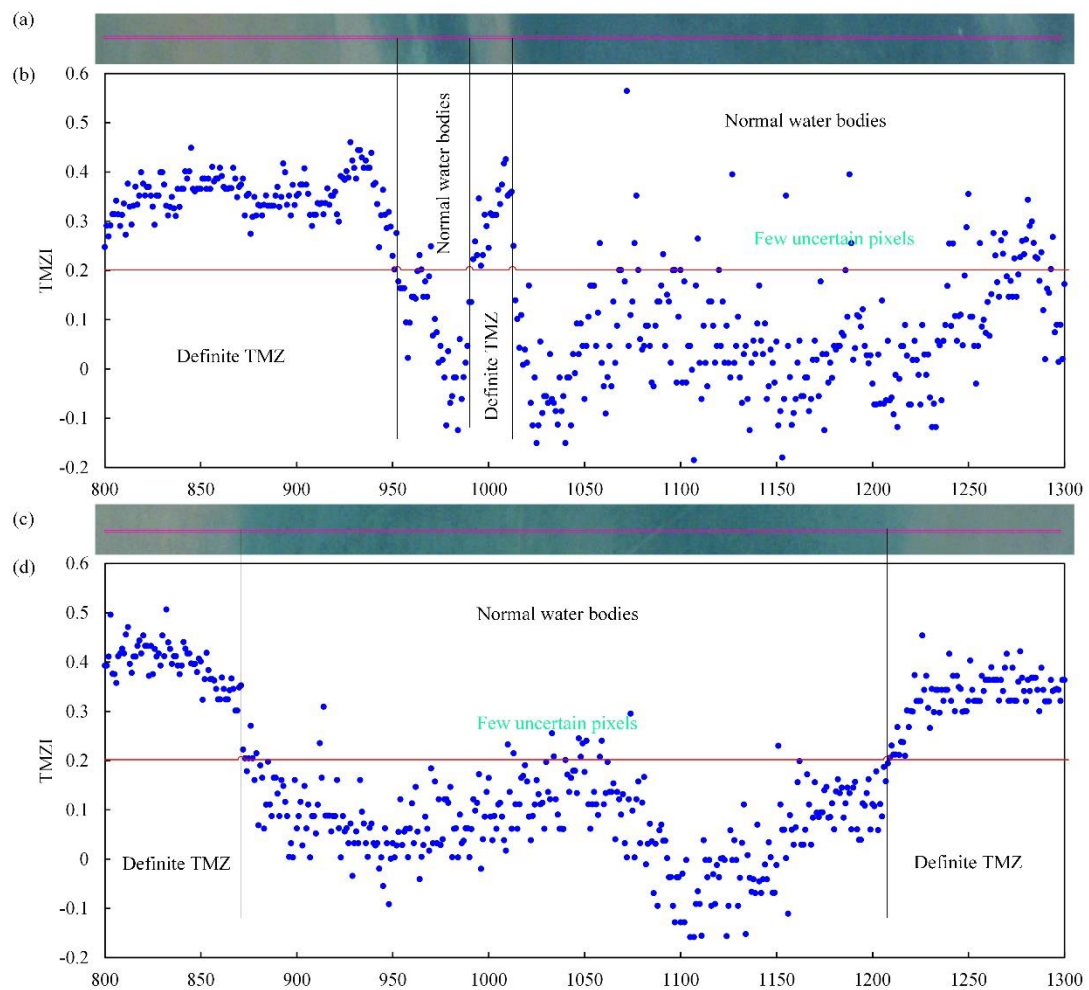
242
$$TMZI = [\text{Log}(TSS) - \text{Log}(Chla)] / [\text{Log}(TSS) + \text{Log}(Chla)] \quad (3)$$



243
 244 **Fig. 5.** The corresponding spatial relationship between the TSS concentrations, indicated by black
 245 dots and red trend line, and Chla concentrations, indicated by green triangles and orange trend line
 246 of row 1600 (a), the true color imagery (b) and the corresponding values of TMZI (c).

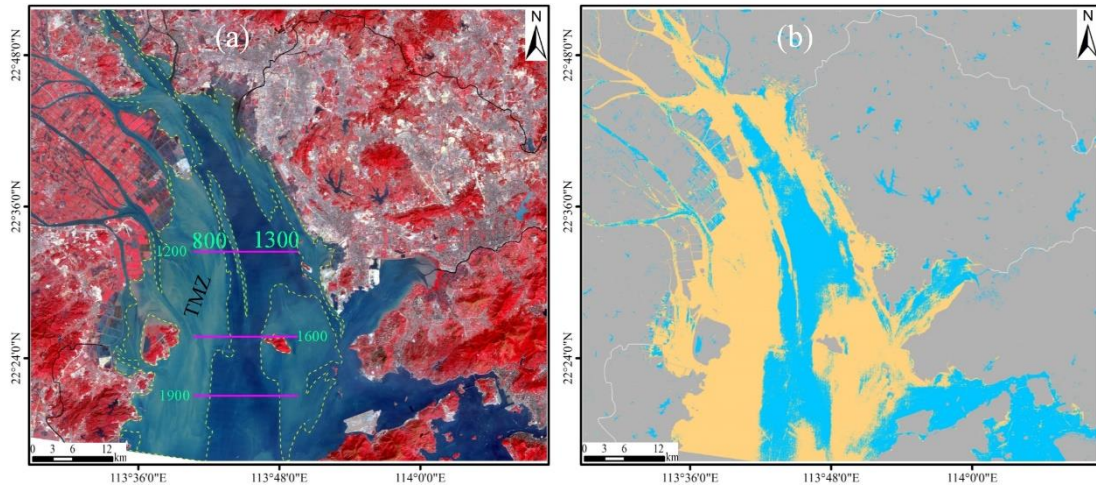
247 According to the definition and equation, this study calculated TMZI values (Figs.
 248 5c, 6b and d). Taking the results of row 1600 as an example (Fig. 5b and c), the row
 249 pixels can be mainly divided into one TMZ (columns 800-975), normal water bodies
 250 (columns 975-1110), and another TMZ (columns 1110-1300) from left to right. The null

251 values located in columns 1180-1200 and 1220-1235 are Neilingding Island (Figs. 5
 252 and 7a). Through a comparison with the results of TMZI, it is found that all the values
 253 of TMZI corresponding to TMZ pixels are larger than 0.2, while the values
 254 corresponding to normal water body pixels are all smaller than 0.2, except for a few
 255 blurry pixels (Figs. 5b and c). For the results of rows 1200 and 1900, similar
 256 corresponding characteristics between TMZ and TMZI and the same criterion were also
 257 found (Fig. 6). Therefore, TMZI showed a significant feature and had the potential to
 258 develop into a better model for recognizing and extracting estuarine TMZ.



259
 260 **Fig. 6.** The true color imagery and the corresponding values of TMZI of rows 1200 (a and b) and
 261 1900 (c and d).

262 The TMZI of the entire Landsat TM imagery was subsequently calculated, and
263 TMZs in the PRE were extracted. [Fig. 7\(b\)](#) shows the spatial distribution results of
264 TMZ in the PRE on November 20, 2004. TMZ is widely distributed throughout the
265 PRE, accounting for more than half of the water areas in the imagery. Among them, the
266 main TMZ is located within an average distance of 11 km from the Panyu, Nansha,
267 Zhongshang, and Zhuhai coasts, which approximately corresponds to the west shoal in
268 the PRE. In the western Dongguan and Shenzhen coastal water bodies, an
269 approximately rectangular TMZ develops approximately 5 km from the coastline,
270 which indicates the location of the east shoal of the PRE ([Wang et al., 2018](#)). In addition,
271 a third main TMZ in the PRE located from surrounding Neilingding Island to western
272 Hong Kong water bodies is found, although TSS concentrations in TMZ are lower than
273 those of the former TMZs ([Figs.4a and 7b](#)). Compared to the visual interpretation of
274 TMZ results in previous works by the current authors ([Fig.7 a](#)) ([Wang et al., 2020b,](#)
275 [2021](#)), the area-based accuracy measures show that the quality of extraction achieves
276 0.8429. The good TMZ extraction results and the high validation accuracy by TMZI in
277 this study indicate a more effective way to recognize TMZs in estuaries ([Figs. 6-7](#)).



278

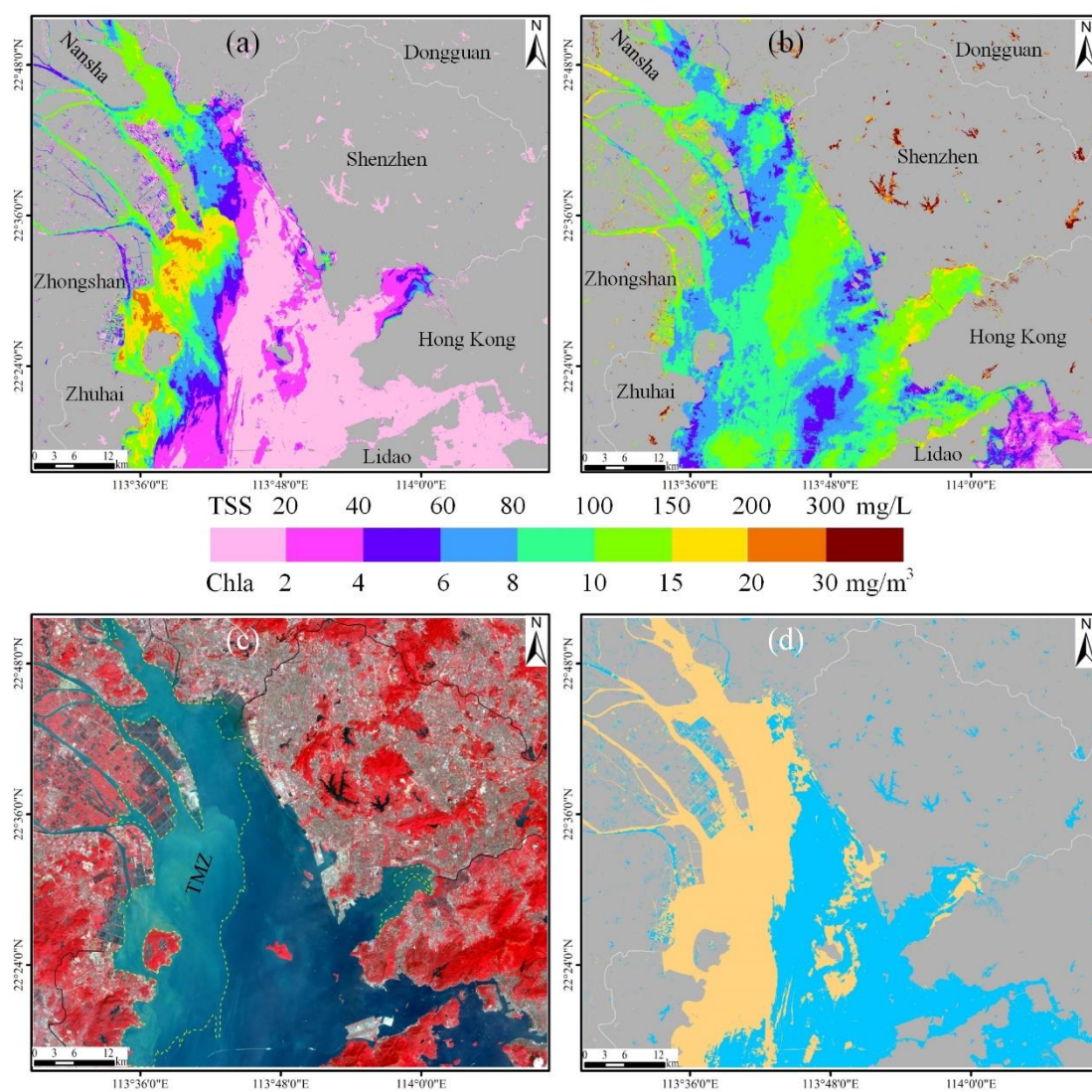
279 **Fig. 7.** False color imagery (USGS 1982; NASA 2001) and the visual interpretation TMZ results
 280 (regions indicated by yellow dashed frames) (Wang et al., 2020b, 2021) (a), and the extracted TMZ
 281 results, indicated by mango colors (b) in the PRE on November 20, 2004 (low-flow season).

282 3.3 Validation of the accuracy of TMZI in different seasons

283 Due to the complexity of hydrodynamic environments, the estuarine factors and
 284 water color elements show significant variations in different seasons, even in the same
 285 estuary at different times of the day. Therefore, this study further validated the accuracy
 286 of TMZI for extracting TMZ in the PRE during the high-flow season (October 18, 2015).

287 Fig. 8(a) and (b) demonstrate the retrieved TSS and Chla concentration results in
 288 the high-flow season of PRE. The results in different seasons are significantly different
 289 (Figs. 4 and 8). On October 18, 2015, TSS concentrations in the PRE had wider
 290 variables, ranging from 2.23 to 286.6 mg/L. However, the water bodies with high TSS
 291 concentrations (more than 80 mg/L) were mainly in the outlets of four waterways,
 292 namely, the Humen, Jiaomen, Hongqimen, and Hengmen waterways. The other regions

293 of the PRE have significantly lower TSS concentrations of generally less than 20 mg/L
 294 (Fig. 8a). Similar to the corresponding features between TSS and Chla concentrations
 295 in the low-flow season, the almost opposite spatial characteristics remain in the high-
 296 flow season. For regions with relatively high (low) Chla concentrations there are
 297 relatively low (high) TSS concentrations (Figs. 8a and b). Notably, the eastern Lidao
 298 district coastal water bodies are an exception, with the same results in the low-flow
 299 season (Fig. 4). Both TSS and Chla concentrations in the zone are relatively low (Figs.
 300 4 and 8).



301

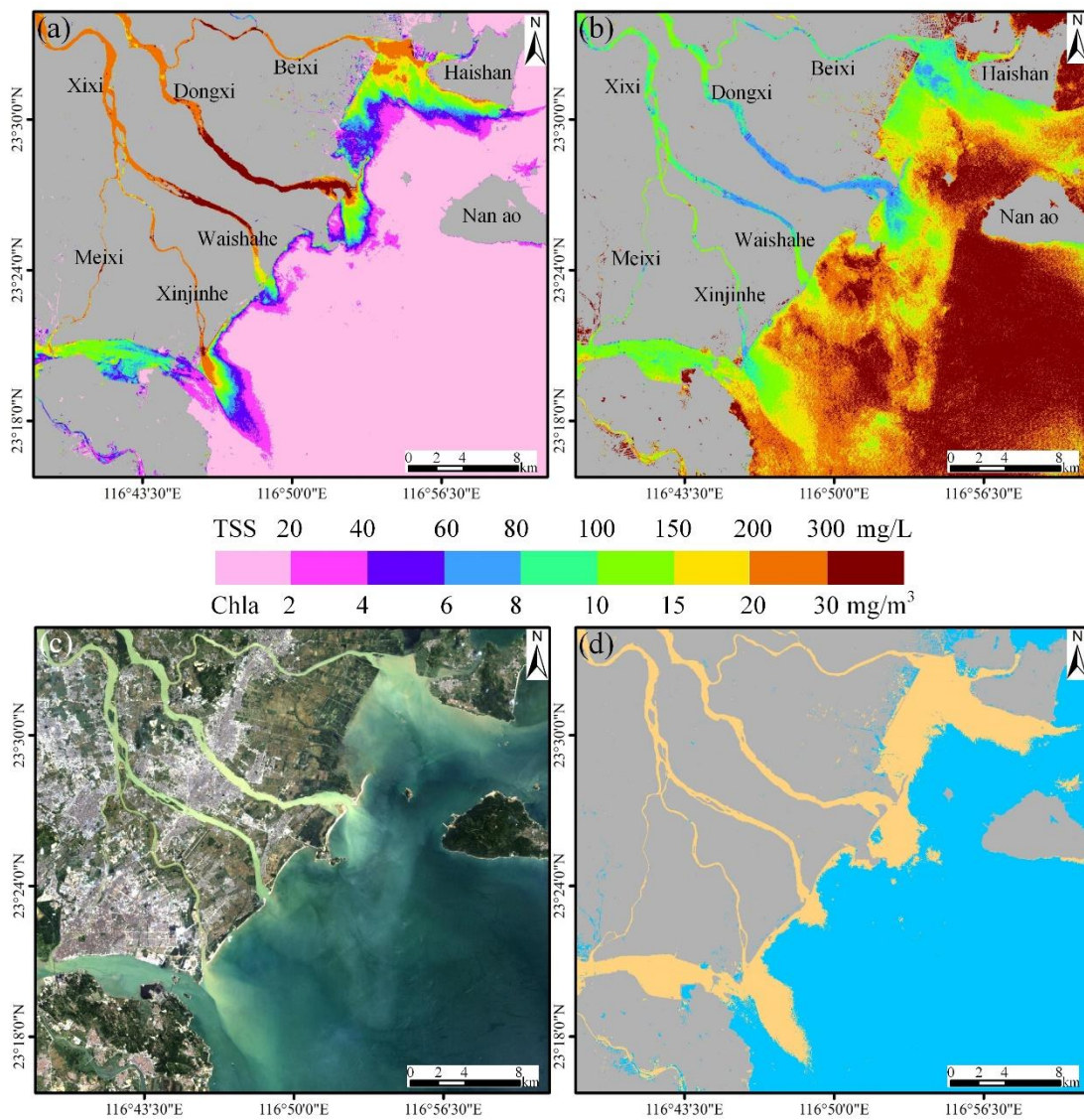
302 **Fig. 8.** The estimated TSS concentrations (a), Chla concentrations (b), false color imagery (USGS
303 1982; NASA 2001), and the visual interpretation TMZ results (regions indicated by yellow dashed
304 frames) (Wang et al., 2020b) (c), and extracted TMZ results, indicated by mango colors mango
305 colors (d) in the PRE on October 18, 2015 (high-flow season).

306 Using the results of TSS and Chla concentrations of the PRE on October 18, 2015,
307 the TMZI was calculated and TMZs of the PRE were extracted in the high-flow season
308 (Fig. 8d). Compared with the visual interpretation TMZ results (Fig.8 c) (Wang et al.,
309 2020b), the area-based accuracy measures show that the quality of extraction is 0.8171.
310 It is also indicated that an acceptable accuracy is obtained by TMZI in the high-flow
311 season of the PRE. In addition, only one main TMZ remains along the west coast of the
312 PRE (Fig. 8d), which is similar to one of the main TMZs in the low-flow season of
313 2004 (Fig. 7b). However, clear differences remain in different seasons, such as TMZs
314 in the Hongqimen and Hengmen waterways and the eastern Zhuhai coasts (Figs. 7b and
315 8d). The other TMZs in the high-flow season of 2015 are mainly located in the
316 surrounding Dachanwan Wharf of Shenzhen and Neilingding Island. The distributions
317 are less apparent than those in the low-flow season of 2004 (Fig. 7b). Besides, two
318 relatively small isolated TMZs can be found on the two artificial islands of the Hong
319 Kong-Zhuhai-Macao Bridge (Fig. 8d), which may imply the associated influence of
320 human activities.

321 According to the analysis of the PRE results on October 18, 2015, it is
 322 demonstrated that the TMZI and the criterion ($TMZI > 0.2$) also perform well in
 323 extracting estuarine TMZ in different seasons using Landsat OLI imagery.

324 3.4 Assessment of the applicability of TMZI in different estuaries

325 To further assess the applicability of TMZI in different estuaries, as for the PRE,
 326 the corresponding TMZ results in the HRE and the MRE were also calculated and
 327 validated.



328

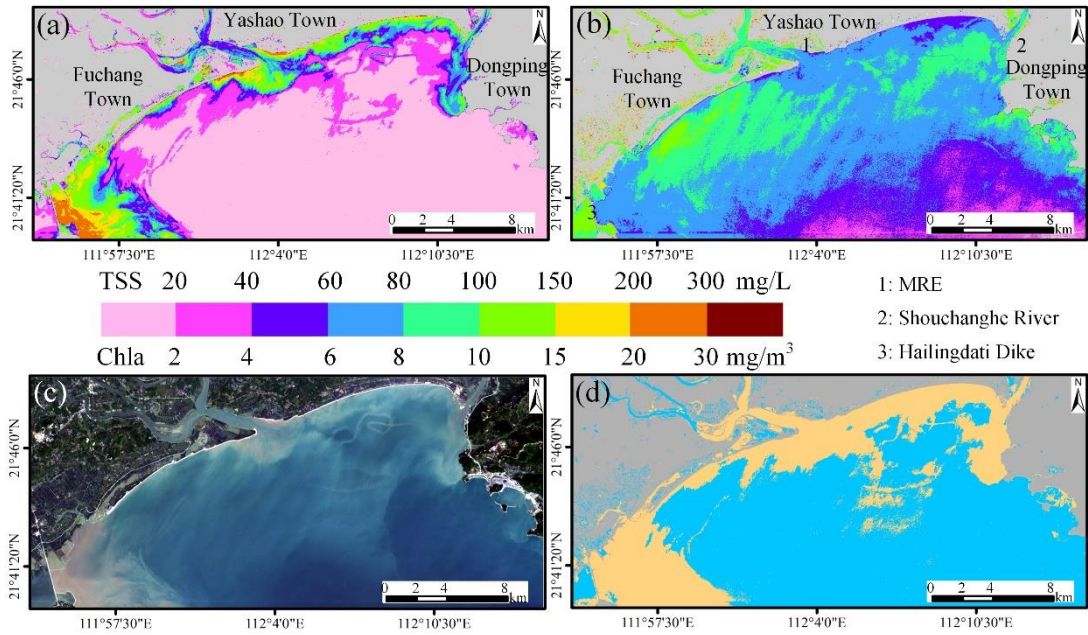
329 **Fig. 9.** The estimated TSS concentrations (a), Chla concentrations (b), true color imagery (USGS
330 1982; NASA 2001) (c), and extracted TMZ results, indicated by mango colors (d) in the HRE on
331 August 13, 2008 (high-flow season).

332 **Fig. 9** (a) and (b) indicate the results of TSS and Chla concentrations in the HRE
333 on August 13, 2008. The TSS concentrations downstream and in the estuary of the HRE
334 are significantly higher than the outer shelf area, particularly in the downstream of the
335 Dongxi River and Xinjinhe River waterways of the Hanjiang River, with a mean value
336 in excess of 300 mg/L (**Fig. 9a**). TSS concentrations in the offshore area (South China
337 Sea) are frequently less than 20 mg/L. Therefore, a significant decreasing trend of TSS
338 concentration is found from the northwest to southeast in the HRE (**Fig. 9a**).
339 Furthermore, the Chla concentrations in the HRE show opposite spatial distributions
340 characteristics, which resembles the findings in the PRE (**Figs. 4 and 8**). Relatively low
341 Chla concentrations are mainly generally found in the downstream and estuary, and the
342 outer shelf area has high values (**Fig. 9b**). The Chla concentrations in the HRE range
343 from 4.1 to 37.3 mg/m³ (**Fig. 9b**), which is slightly higher than that of the PRE (**Figs. 4**
344 **and 8**).

345 The TMZ extraction results for the HRE are shown in **Fig. 9(d)**. The TMZs are
346 distributed in all the downstream and estuaries of the Hangjiang River. They can be
347 divided into four main TMZs based on different waterways, namely, the Beixi, Dongxi,
348 Waishahe, Xinjinhe, and Meixi waterways of the Hanjing River. The maximum TMZ
349 is located within an average distance of 3 km from the Beixi estuary, western Haishan

350 coast, and the coastlines between the Beixi and Dongxi estuaries. The second largest
351 TMZ of the HRE is distributed from the Meixi to the Xinjinhe estuaries. The region of
352 the main TMZ of the Xinjinhe estuary appears knife-shaped, which is mainly caused
353 by the runoff of the Xinjinhe waterway and the flow guiding line connected to Longhu
354 District, Shantou City (Fig. 9 d) (Wang et al., 2017a). The other two relatively smaller
355 TMZs are distributed in the Dongxi and Waishahe estuaries, respectively. The results
356 indicate that the TMZ distribution in the HRE is mainly related to tide, runoff, estuarine
357 topography, and human activity.

358 In the MRE, the region of high TSS concentrations is mainly distributed at an
359 average distance of 1.2 km from the Yangjiang coastlines, particularly in the eastern
360 Hailingdati dike water bodies, with a mean value of more than 150 mg/L (Fig. 10a).
361 The outer shelf area has significantly lower TSS concentrations of generally less than
362 35 mg/L. The Chla concentrations in most regions of the MRE are more than 4 mg/m³,
363 except for the southwestern Dongping town coastal water bodies, where Chla
364 concentrations mainly range from 2 to 4 mg/m³. The Chla concentrations in the
365 Moyangjiang River downstream, Fuchang town coast, and outside of the Shouchanghe
366 River estuary have relatively high values of frequently greater than 8 mg/m³ (Fig. 10b).
367 Compared to the PRE and the HRE, the corresponding relationship between TSS and
368 Chla concentrations in the MRE is slightly weak. However, a trend of high (low) TSS
369 concentrations in water bodies with relatively low (high) Chla concentrations remains
370 (Figs. 10a and b).



371

372 **Fig. 10.** The estimated TSS concentrations (a), Chla concentrations (b), true color imagery (USGS
 373 1982; NASA 2001) (c), and extracted TMZ results, indicated by mango colors (d) in the MRE on
 374 December 6, 2013 (Low-flow season).

375 **Figs. 10** (c) and (d) indicate the true color imagery of the MRE and the TMZs
 376 extraction results. There are two main TMZs in the MRE on December 6, 2013. The
 377 first TMZ is mainly distributed from the inside and outside of the Moyangjiang River
 378 estuary to the Shouchanghe River estuary, with a distance of approximately 1.8 km
 379 from the coastlines (**Fig. 10d**). The distribution of TMZ in this region is mainly
 380 attributed to the interaction of tide and runoff. Another main TMZ is in the regions 4
 381 km from the Hailingdati dike, and is mainly caused by obstruction against ocean
 382 currents (**Fig. 10d**). In addition, several small, long, and narrow TMZs are accuracy
 383 extracted through TMZI with the same criterion as that in the PRE and the HRE.

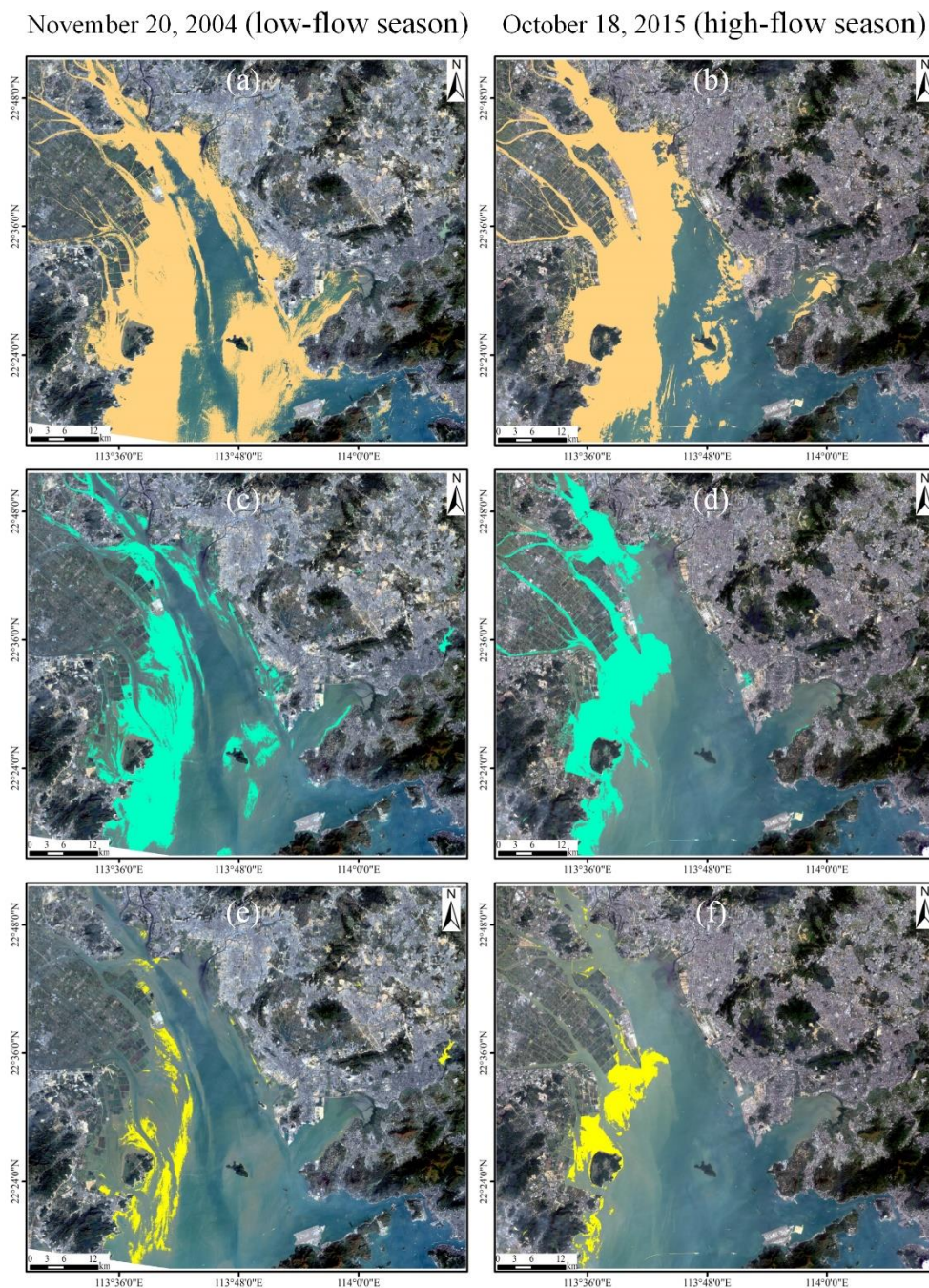
384 The results of the three estuaries and the comparison and accuracy assessment
385 indicate that extracting TMZ based on TMZI and the criterion ($TMZI > 0.2$) has a high
386 applicability in multiple estuaries and different seasons.

387 **3.5 Comparison with the previous methods**

388 Previous studies have extracted TMZ based mainly on the threshold of TSS
389 concentrations or turbidity. For example, [Jalón-Rojas et al. \(2016\)](#) used thresholds of
390 500 mg/L (300 NTU) and 1000 mg/L (600 NTU) to define moderately concentrated
391 TMZ and highly concentrated TMZ in the Loire Estuary in France; [Jiang et al. \(2013\)](#)
392 and [Li et al. \(2019\)](#) defined TMZ as the areas with TSS values larger than 700 mg/L in
393 Yangtze Estuary and Hangzhou Bay. For TMZ in the PRE, it was found that TSS values
394 in studies by [Shi et al. \(2017\)](#) and [Wai et al. \(2004\)](#) were more than 89.4 mg/L and
395 about 150 mg/L, respectively. Based on the two criteria (TMZ: $TSS > 89.4$ mg/L or
396 $TSS > 150$ mg/L), this study calculated and extracted TMZs in the PRE ([Fig. 11c-f](#)).

397 Compared to the visual interpretation TMZ results ([Figs. 7a and 8c](#)), the TMZ
398 extraction results in the PRE based on the criterion of [Shi et al. \(2017\)](#) are superior to
399 those of [Wai et al. \(2004\)](#), on November 20, 2004 ([Fig. 11c vs. Fig. 11e](#), low-flow
400 season) or October 18, 2015 ([Fig. 11d vs. Fig. 11f](#), high-flow season). The extraction
401 quality based on the criteria of [Shi et al. \(2017\)](#) and [Wai et al. \(2004\)](#) are 0.4238, 0.4770
402 and 0.1046, 0.1661, respectively. The primary reason may be that the time of the data
403 source in [Shi et al. \(2017\)](#) was closer to the present study than that in the study by [Wai](#)

404 [et al. \(2004\)](#). This means that the criterion of [Shi et al. \(2017\)](#) was more suitable for this
405 study than that of [Wai et al. \(2004\)](#).



407 **Fig. 11.** The true color imagery (USGS 1982; NASA 2001) and TMZ extraction results in the PRE
408 at different time (a, c, e: November 20, 2004; b, d, f: October 18, 2015) based on the TMZI method
409 of this study (a and b, regions indicated by mango color, as in [Fig. 7b](#) and [Fig. 8d](#)), the criterion by

410 [Shi et al. \(2017\)](#) (c and d, regions indicated by cyan color), and the criterion by [Wai et al. \(2004\)](#) (e
411 and f, regions indicated by yellow color).

412 It was also found that a relatively good result was obtained in the west shoal of the
413 PRE on November 20, 2004, according to the criterion of [Shi et al. \(2017\)](#) ([Fig. 11c](#)).
414 The extracted TMZs are almost consistent with the reality compared to the true color
415 imagery and the visual interpretation TMZ results ([Wang et al., 2020b, 2021](#)). However,
416 the accuracy in the east shoal and surrounding Neilingding Island of the PRE is lower
417 than in the west shoal, where obvious distributions of TMZs are not recognized
418 effectively ([Fig. 11c](#)). Furthermore, the same criterion does not work well in the western
419 shoal of the PRE at different times ([Fig. 11c](#) vs. [Fig. 11d](#)). Almost one-third of the
420 distributions of TMZs in the western shoal of the PRE during the high-flow season are
421 not distinguished and extracted ([Fig. 11d](#)). The results based on the criteria of previous
422 studies, indicate that fixed thresholds have a distinct disadvantage when extracting
423 TMZ at different times or in estuaries.

424 Based on the evaluation and analysis of all the above results ([Figs. 7-11](#)), TMZI
425 could be widely and effectively applied for the accurate extraction of estuarine TMZ,
426 regardless of the significant variations in hydrodynamic environments, TSS and Chla
427 concentrations in different estuaries and seasons. Compared to previous studies and the
428 results from fixed thresholds, it is concluded that TMZI has significant potential to
429 develop into a unified model for distinguishing and extracting TMZ effectively and
430 accurately in many other estuaries globally (Q: 0.8171-0.8429 vs. 0.1046-0.4770).

431 **4 Summary and Conclusions**

432 This study established and developed a novel model (turbidity maximum zone
433 index) based on TSS and Chla concentration, to distinguish estuarine turbidity
434 maximum zone from Landsat imageries. It was found that both TSS and Chla
435 concentrations showed significant variations and different characteristics in the PRE,
436 the HRE and the MRE in different times (Figs. 4 and 8-10). A corresponding
437 relationship between TSS and Chla concentrations in the three estuaries of Guangdong
438 Province remains. In this study, the Chla and TSS concentrations showed almost
439 opposite spatial distribution characteristics, where relatively high (low) Chla
440 concentrations corresponded exactly to the relatively low (high) TSS concentrations
441 (Figs. 4-5 and 8-10). Therefore, here, the turbidity maximum zone index (TMZI) was
442 defined and designed as the ratio of the difference and sum of the logarithmic
443 transformation of TSS and Chla concentrations.

444 Compared with the true (false) color imagery and the visual interpretation TMZ
445 results, it was found that the TMZ extraction results by TMZI were consistent with the
446 reality (Figs. 7-10; Q: 0.8171-0.8429). Notably, the criterion used for extracting TMZs
447 in different estuaries and seasons was the same ($TMZI > 0.2$). In addition, reasonable
448 accuracy and a better performance were obtained by TMZI compared with the previous
449 fixed TSS concentration or turbidity threshold (Fig. 11; Q: 0.8171-0.8429 vs. 0.1046-
450 0.4770), demonstrating that TMZI has a higher adaptability and robustness.

451 The results of this study indicate that there is significant potential for optimizing
452 TMZI to distinguish and extract TMZs from multi-source satellite remote sensing, such
453 as Sentinel, Aqua & Terra-MODIS, Envisat MERIS and SeaWiFS. This will also assist
454 in establishing and developing a global unified criterion for extracting TMZs effectively
455 in different estuaries and at different times.

456 **Code and data availability**

457 All the Landsat remote sensing imageries are fully available at
458 <https://glovis.usgs.gov/> (USGS 1982; NASA 2001).

459 **Author Contributions**

460 The individual contributions and responsibilities of the authors are listed as
461 follows: CW designed the research and wrote the paper; CZ, DL and LW guided the
462 research process; DW, QZ, HJ, KJ and YL collected and analyzed the data; SCh, JY,
463 XZ and YL revised the manuscript, provided some comments and helped edit the
464 manuscript. All authors have read and agreed to the published version of the manuscript.

465 **Competing interests**

466 The authors declare that they have no conflict of interest.

467 **Acknowledgements**

468 This work was funded jointly by National Natural Science Foundation of China
469 (41801364 and 41976189), Natural Science Foundation of Guangdong Province
470 (2021A1515012579), Key Special Project for Introduced Talents Team of Southern
471 Marine Science and Engineering Guangdong Laboratory (Guangzhou)
472 (GML2019ZD0301), Guangdong Innovative and Entrepreneurial Research Team
473 Program (2016ZT06D336) and GDAS' Project of Science and Technology
474 Development (2020GDASYL-20200104006, 2020GDASYL-20200302001 and
475 2019GDASYL-0301001). We would also like to thank USGS for providing the Landsat
476 remote sensing imageries.

477 **Review statement**

478 This paper was edited by Richard Neale and reviewed by two anonymous referees.

479 **References**

480 Asp, N.E., Gomes, V., Schettini, C.A.F., Filho, P.W.S., Siegle, E., Ogston, A.s.,
481 Nittrouer, C.A., Silva, J.N.S., Nascimento, W.R., Jr, Souza, S.R., Pereira, L.C.C.,
482 and Queiroz, M.C.: Sediment dynamics of a tropical tide-dominated estuary:
483 Turbidity maximum, mangroves and the role of the Amazon River sediment load.
484 Estuarine, Coastal and Shelf Science. 214, 10-24,
485 <https://doi.org/10.1016/j.ecss.2018.09.004>, 2018.

486 Attila, J., Kauppila, P., Kallio, K.Y., Alasalmi, H., Keto, V., Bruun, E., and Koponen,
487 S.: Applicability of Earth Observation chlorophyll-a data in assessment of water
488 status via MERIS-With implications for the use of OLCI sensor. *Remote Sensing*
489 *of Environment*. 212, 273-287, <https://doi.org/10.1016/j.rse.2018.02.043>, 2018.

490 Azhikodan, G. and Yokoyama, K.: Seasonal morphodynamic evolution in a meandering
491 channel of a macrotidal estuary. *Science of the Total Environment*. 684, 281-295,
492 <https://doi.org/10.1016/j.scitotenv.2019.05.289>, 2019.

493 Brenon, I. and Hir, P.L.: Modelling the Turbidity Maximum in the Seine Estuary
494 (France): Identification of Formation Processes. *Estuarine, Coastal and Shelf*
495 *Science*. 49, 525-544, <https://doi.org/10.1006/ecss.1999.0514>, 1999.

496 Cai, L., Shi, W., Miao, Z., and Hao, M.: Accuracy Assessment Measures for Object
497 Extraction from Remote Sensing Images. *Remote Sensing*, 10, 303,
498 <https://doi.org/10.3390/rs10020303>, 2018.

499 Chen, S., Fang, L., Li, H., Chen, W., and Huang, W.: Evaluation of a three-band model
500 for estimating chlorophyll-a concentration in tidal reaches of the Pearl River
501 Estuary, China. *ISPRS Journal of Photogrammetry and Remote Sensing*. 68, 356-
502 364, <https://doi.org/10.1016/j.isprsjprs.2011.01.004>, 2011.

503 Chen, S., Han, L., Chen, X., Li, D., Sun, L., and Li, Y.: Estimating wide range Total
504 Suspended Solids concentrations from MODIS 250-m imageries: An improved
505 method. *ISPRS Journal of Photogrammetry and Remote Sensing*. 99, 58-69,
506 <https://doi.org/10.1016/j.isprsjprs.2014.10.006>, 2015.

507 Chen, X., Shen, Z., and Yang, Y.: Response of the turbidity maximum zone in the
508 Yangtze River Estuary due to human activities during the dry season.
509 Environmental Science and Pollution Research. 11, 1-16,
510 <https://doi.org/10.1007/s11356-016-6872-1>, 2016.

511 Feng, H., Cochran, J.K., and Hirschberg, D.J.: Transport and sources of metal
512 contaminants over the course of tidal cycle in the turbidity maximum zone of the
513 Hudson River estuary. Water Research. 36, 733-743,
514 [https://doi.org/10.1016/S0043-1354\(01\)00268-8](https://doi.org/10.1016/S0043-1354(01)00268-8), 2002.

515 Gebhardt, A.C., Schoster, F., Gaye-Haake, B., Beeskow, B., Rachold, V., Unger, D.,
516 and Ittekkot, V.: The turbidity maximum zone of the Yenisei River (Siberia) and
517 its impact on organic and inorganic proxies. Estuarine, Coastal and Shelf Science.
518 65, 61-73, <https://doi.org/10.1016/j.ecss.2005.05.007>, 2005.

519 Gong, S., Gao, A., Lin, J., Zhu, X., Zhang, Y., and Hou, Y.: Temporal-spatial
520 distribution and its influencing factors of suspended particulate matters in
521 Minjiang lower reaches and estuary. Journal of Earth Sciences and Environment.
522 39(6), 826-836, [doi:1672-6561\(2017\)06-0826-11](https://doi.org/10.1016/j.ecss.2017.06.0826-11), 2017.

523 Grasso, F., Verney, R., Hir, P.L., Thouvenin, B., Schulz, E., Kervella, Y., Fard, I.K.P.,
524 Lemoine, J.-P., Dumas, F., and Garnie, V.: Suspended Sediment Dynamics in the
525 Macrotidal Seine Estuary (France) - Part 1: Numerical Modeling of Turbidity
526 Maximum Dynamics. Journal of Geophysical Research: Oceans. 123, 558-577,
527 <https://doi.org/10.1002/2016JC012638>, 2018.

528 Gregg, W.W. and Casey, N.W.: Global and regional evaluation of the SeaWiFS
529 chlorophyll data set. *Remote Sensing of Environment*. 93, 463-479,
530 <https://doi.org/10.1016/j.rse.2003.12.012>, 2004.

531 Huang, B., Hong, H., Ke, L., and Cao, Z.: Size-fractionated phytoplankton biomass and
532 productivity in the Zhujiang River Estuary in China. *Acta Oceanologica Sinica*.
533 27, 180-186, [doi:10.1016/j.aos.2005.06.018](https://doi.org/10.1016/j.aos.2005.06.018), 2005.

534 Jalón-Rojas, I., Schmidt, S., Sottolichio, A., and Bertier, C.: Tracking the turbidity
535 maximum zone in the Loire Estuary (France) based on a long-term, high-
536 resolution and high-frequency monitoring network. *Continental Shelf Research*.
537 117, 1-11, <https://doi.org/10.1016/j.csr.2016.01.017>, 2016.

538 Jiang, J., He, Q., Zhu, L., and Lin, J.: Analysis of hydrodynamic features of the North
539 Passage in the turbidity maximum, Changjinag Estuary. *Haiyang Xuebo*. 41(1),
540 11-20, [doi:10.3969/j.issn.0253-4193.2019.01.002](https://doi.org/10.3969/j.issn.0253-4193.2019.01.002), 2019.

541 Jiang, X., Lu, B., and He, Y.: Response of the turbidity maximum zone to fluctuations
542 in sediment discharge from river to estuary in the Changjiang Estuary (China).
543 *Estuarine, Coastal and Shelf Science*. 131, 24-30,
544 <https://doi.org/10.1016/j.ecss.2013.07.003>, 2013.

545 Kim, H.H., Ko, B.C., and Nam, J.Y.: Predicting chlorophyll-a using Landsat 8 OLI
546 sensor data and the non-linear RANSAC method-a case study of Nakdong River,
547 South Korea. *International Journal of Remote Sensing*. 37, 3255-3271,
548 <https://doi.org/10.1080/01431161.2016.1196839>, 2016a.

549 Kim, W., Moon, J.-E., Park, Y.-J., and Ishizaka, J.: Evaluation of chlorophyll retrievals
550 from Geostationary Ocean Color Imager (GOCI) for the North-East Asian region.
551 Remote Sensing of Environment. 184, 482-495,
552 <https://doi.org/10.1016/j.rse.2016.07.031>, 2016b.

553 Kitheka, J.U., Mavuti, K.M., Nthenge, P., and Obiero, M.: The turbidity maximum zone
554 in a shallow, well-flushed Sabaki estuary in Kenya. Journal of Sea Research. 110,
555 17-28, <https://doi.org/10.1016/j.seares.2015.03.001>, 2016.

556 Le, C., Hu, C., Cannizzaro, J., English, D., Muller-Karger, F., and Lee, Z.: Evaluation
557 of chlorophyll-a remote sensing algorithms for an optically complex estuary.
558 Remote Sensing of Environment. 129, 75-89,
559 <https://doi.org/10.1016/j.rse.2012.11.001>, 2013.

560 Le, C., Li, Y., Zha, Y., Sun, D., Huang, C., and Lu, H.: A four-band semi-analytical
561 model for estimating chlorophyll a in highly turbid lakes: The case of Taihu Lake,
562 China. Remote Sensing of Environment. 113, 1175-1182,
563 <https://doi.org/10.1016/j.rse.2009.02.005>, 2009.

564 Li, L., Ye, T., Wang, X., and Xia, Y.: Tracking the multidecadal variability of the surface
565 turbidity maximum zone in Hangzhou Bay, China. International Journal of Remote
566 Sensing. 1-22, <https://doi.org/10.1080/01431161.2019.1633701>, 2019.

567 Liu, H., Huang, L., Tan, Y., Ke, Z., Liu, J., Zhao, C., and Wang, J.: Seasonal variations
568 of chlorophyll a and primary production and their influencing factors in the Pearl

569 River Estuary. *Journal of Tropical Oceanography*. 36, 81-91,
570 [doi:10.11978/2016033](https://doi.org/10.11978/2016033), 2017.

571 Liu, R., Wang, Y., Gao, J., Wu, Z., and Guan, W.: Turbidity maximum formation and
572 its seasonal variations in the Zhujiang (Pearl River) Estuary, southern China. *Acta*
573 *Oceanologica Sinica*. 35, 22-31, <https://doi.org/10.1007/s13131-016-0897-7>, 2016.

574 Mitchell, S. B.: Turbidity maxima in four macrotidal estuaries. *Ocean & Coastal*
575 *Management*. 79, 62-69, <https://doi.org/10.1016/j.ocecoaman.2012.05.030>, 2013.

576 Mitchell, S., Akesson, L., and Uncles, R.: Observations of turbidity in the Thames
577 Estuary, United Kingdom. *Water and Environment Journal*. 26, 511-520,
578 <https://doi.org/10.1111/j.1747-6593.2012.00311.x>, 2012.

579 Montanher, O., Novo, E., Barbosa, C., Renno, C., and Silva, T.: Empirical models for
580 estimating the suspended sediment concentration in Amazonian white water rivers
581 using Landsat 5/TM. *International Journal of Applied Earth Observation and*
582 *Geoinformation*, 29, 67-77, <https://doi.org/10.1016/j.jag.2014.01.001>, 2014.

583 Park, K., Wang, H.V., Kim, S.-C., and Oh, J.-H.: A Model Study of the Estuarine
584 Turbidity Maximum along the Main Channel of the Upper Chesapeake Bay.
585 *Estuaries and Coasts*. 31, 115-133, <https://doi.org/10.1007/s12237-007-9013-8>,
586 2008.

587 Pozdnyakov, D., Shuchman, R., Korosov, A., and Hatt, C.: Operational algorithm for
588 the retrieval of water quality in the Great Lakes. *Remote Sensing of Environment*.
589 97, 352-370, <https://doi.org/10.1016/j.rse.2005.04.018>, 2005.

590 Schubel, J.: Turbidity maximum of the northern chesapeake bay. SCIENCE. 161, 1013-
591 1015, [doi:10.1126/science.161.3845.1013](https://doi.org/10.1126/science.161.3845.1013), 1968.

592 Shen, H.: New understanding on the study of the maximum turbidity zone in estuaries
593 of China. Advence in Earth Sciences. 10, 210-212, [doi: 10.11867/j.issn.1001-
594 8166.1995.02.0210](https://doi.org/10.11867/j.issn.1001-8166.1995.02.0210), 1995.

595 Shen, H., He, S., Mao, Z., and Li, J.: On the turbidity maximum in the Chinese estuaries.
596 Journal of Sediment Research. 1, 23-29. [doi : 10.3321/j.issn:0468-
597 155X.2001.01.004](https://doi.org/10.3321/j.issn:0468-155X.2001.01.004), 2001.

598 Shi, W., Shen, H., and Li, J.: Review on the formation of estuarine turbidity maximum.
599 Advence in Earth Sciences. 8, 8-13, [doi:CNKI:SUN:DXJZ.0.1993-01-001](https://doi.org/CNKI:SUN:DXJZ.0.1993-01-001), 1993.

600 Shi, Z., Xu, J., Huang, X., Zhang, X., Jiang, Z., Ye, F., and Liang, X.: Relationship
601 between nutrients and plankton biomass in the turbidity maximum zone of the
602 Pearl River Estuary. Journal of Environmental Sciences. 57, 72-84,
603 <https://doi.org/10.1016/j.jes.2016.11.013>, 2017.

604 Song, K., Li, L., Tedesco, L.P., Li, S., Duan, H., Liu, D., Hall, B.E., Du, J., Li, Z., Shi,
605 K., and Zhao, Y.: Remote estimation of chlorophyll-a in turbid inland waters:
606 Three-band model versus GA-PLS model. Remote Sensing of Environment. 136,
607 342-357, <http://dx.doi.org/10.1016/j.rse.2013.05.017>, 2013.

608 Toubanc, F., Brenon, I., and Coulombier, T.: Formation and structure of the turbidity
609 maximum in the macrotidal Charente estuary (France)_ Influence of fluvial and

610 tidal forcing. *Estuarine, Coastal and Shelf Science*. 169, 1-14,
611 <https://doi.org/10.1016/j.ecss.2015.11.019>, 2016.

612 Uncles, R.J., Bloomer, N.J., Frickers, P.E., Griffiths, M.L., Harris, C., Howland, R.J.M.,
613 Morris, A.W., Plummer, D.H., and Tappin, A.D.: Seasonal variability of salinity,
614 temperature, turbidity and suspended chlorophyll in the Tweed Estuary. *Science*
615 *of the Total Environment*. 251/252, 115-124, [https://doi.org/10.1016/S0048-](https://doi.org/10.1016/S0048-9697(00)00405-8)
616 [9697\(00\)00405-8](https://doi.org/10.1016/S0048-9697(00)00405-8), 2000.

617 Wai, O.W.H., Wang, C., Li, Y., and Li, X.: The formation mechanisms of turbidity
618 maximum in the Pearl River estuary, China. *Marine Pollution Bulletin*. 48, 441-
619 448, [doi:10.1016/j.marpolbul.2003.08.019](https://doi.org/10.1016/j.marpolbul.2003.08.019), 2004.

620 Wan, Y. and Wang, L.: Numerical investigation of the factors influencing the vertical
621 profiles of current, salinity, and SSC with in a turbidity maximum zone.
622 *International Journal of Sediment Research*. 32, 20-33,
623 <https://doi.org/10.1016/j.ijsrc.2016.07.003>, 2017.

624 Wang, C., Chen, S., Li, D., Wang, D., liu, W., and Yang, J. A Landsat-based model for
625 retrieving total suspended solids concentration of estuaries and coasts in China.
626 *Geoscientific Model Development*. 10, 4347-4365, [https://doi.org/10.5194/gmd-](https://doi.org/10.5194/gmd-10-4347-2017)
627 [10-4347-2017](https://doi.org/10.5194/gmd-10-4347-2017), 2017a.

628 Wang, C., Chen, S., Yang, J., Li, Y., Zhou, X., Li, D., and Wang, D.: Monitoring total
629 suspended solids concentrations in estuaries based on remote sensing. Beijing:
630 China Water & Power Press. 2020a.

631 Wang, C., Li, D., Wang, D., and Chen, S.: Detecting the Temporal and Spatial Changes
632 of Suspended Sediment Concentration in Hanjiang River Estuary During the Past
633 30 Years Using Landsat Imageries. *Research Journal of Environmental Science*.
634 11, 143-155, [doi:10.3923/rjes.2017.143.155](https://doi.org/10.3923/rjes.2017.143.155), 2017b.

635 Wang, C., Li, W., Chen, S., Li, D., Wang, D., and Liu, J.: The spatial and temporal
636 variation of total suspended solid concentration in Pearl River Estuary during
637 1987–2015 based on remote sensing. *Science of the Total Environment*. 618, 1125-
638 1138, <https://doi.org/10.1016/j.scitotenv.2017.09.196>, 2018.

639 Wang, C., Wang, D., Yang, J., Fu, S., and Li, D.: Suspended Sediment within Estuaries
640 and along Coasts: A Review of Spatial and Temporal Variations based on Remote
641 Sensing. *Journal of Coastal Research*. 36, 1323-1331,
642 doi.org/10.2112/JCOASTRES-D-19-00164.1, 2020b.

643 Wang, C., Zhou, C., Chen, S., Xie, Y., Li, D., Yang, J., Zhou, X., Li, Y., Wang, D., and
644 Liu, Y.: Retrospect and perspective of the estuarine turbidity maximum zone
645 researches. *Chinese Science Bulletin*. 66, 2328-2342, [doi:10.1360/TB-2020-0938](https://doi.org/10.1360/TB-2020-0938),
646 2021.

647 Yan, D., Song, D., Bao, X.: Spring-neap tidal variation and mechanism analysis of the
648 maximum turbidity in the Pearl River Estuary during flood season. *Journal of*
649 *Tropical Oceanography*. 39, 20-35, [doi:10.11978/2019035](https://doi.org/10.11978/2019035), 2020.

650 Yang, J. and Liu, W.: Characteristics of the maximum turbidity zone in the
651 lingdingyang-Pearl river estuary during the flood season in the recent 30 years.

652 Pearl River Water Transport. 16, 58-62, [doi:10.14125/j.cnki.zjsy.2015.16.034](https://doi.org/10.14125/j.cnki.zjsy.2015.16.034),
653 [2015](https://doi.org/10.14125/j.cnki.zjsy.2015.16.034).

654 Yang, Y., Li, Y., Sun, Z., and Fan, Y.: Suspended sediment load in the turbidity
655 maximum zone at the Yangtze River Estuary: The trends and causes. Journal of
656 Geographical Sciences. 24, 129-142, [doi: 10.1007/s11442-014-1077-3](https://doi.org/10.1007/s11442-014-1077-3), 2014.

657 Yu, Q., Wang, Y., Gao, J., Gao, S., and Flemming, B.: Turbidity maximum formation
658 in a well-mixed macrotidal estuary: The role of tidal pumping. Journal of
659 Geophysical Research: Oceans. 119, 7705-7724,
660 <https://doi.org/10.1002/2014JC010228>, 2014.

661 Zhang, X., Chen, X., Dou, X., Zhao, X., Xia, W., Jiao, J., and Xu, H.: Study on
662 formation mechanism of turbidity maximum zone and numerical simulations in
663 the macro tidal estuaries. Advances in Water Science. 30, 84-92,
664 [doi:10.14042/j.cnki.32.1309.2019.01.009](https://doi.org/10.14042/j.cnki.32.1309.2019.01.009), 2019.